Machine learning applied to automated orbit control at the 1.5–GeV electron storage ring DELTA

D. Schirmer*
TU Dortmund University, Center for Synchrotron Radiation (DELTA), D-44227 Dortmund, Germany
(Dated: September 12, 2021)

Machine learning (ML) methods have found their application in a wide range of particle accelerator control tasks. Among other possible use cases, like anomaly detection and time series studies, neural networks (NNs) can also be utilized for automated beam position control (orbit correction). ML studies on this topic, which were initially based on simulations, were successfully transferred to real accelerator operation. For this purpose, classical fully-connected multi-layer feed-forward NNs were trained by supervised learning on measured orbit data to apply local and global beam position corrections at the 1.5–GeV electron storage ring of the DELTA accelerator facility. The supervised NN training was carried out with various conjugate gradient backpropagation learning algorithms. Afterwards, the ML-based orbit correction (OC) performance was compared with a conventional numerical-based computing method. Here, the ML-based approach showed a competitive orbit correction quality in fewer number of correction steps which yields in a faster OC convergence. This paper summarizes the basic ideas, presents the latest results and points out possible future improvements.

I. INTRODUCTION

Artificial intelligence (AI) is expected to revolutionize many aspects of society and science through its ability to optimize processes and decisions using computer-based algorithms. Machine learning (ML) as a sub-field of AI is based on computational statistical algorithms that allow computers to learn directly from data, without being explicitly programmed. Thus, for example, machine learning techniques have the potential to perform essential tasks of automated controls in particle accelerators. The potential applications of ML in accelerator controls are diverse. They range from automated machine tuning, beam diagnostics, (big) data analysis for fault detection, prediction and classification up to accelerator modeling and simulation [1, 2].

Stable electron orbit control is also an important task especially for modern synchrotron light sources, since uncorrected beam orbits imply large beam amplitudes and angles. This could result in vacuum chamber heating, lower synchrotron radiation beamline illumination, reduced injection efficiency as well as decreased dynamic aperture and hence lower beam lifetime. Therefore, since 2018 [3], ML-based orbit correction (OC) methods have extensively been studied and applied at DELTA, a 1.5-GeV electron storage ring operated as a synchrotron light source and a new facility for ultrashort pulses in the VUV and THz regime [4–6].

In the past, ML techniques were successfully applied to real machine operation for each orbit plane independently [7]. Now, the method has been extended to full x,z-coupled machine operation including weighted beam position monitor (BPM) signals applied to both orbit planes simultaneously. The residual weighted orbit quality has been bench-marked against alternative OC approaches like standard singular value decomposition (SVD) [8–10] and more sophisticated qp-cone-based approaches [11, 12].

* detlev.schirmer@tu-dortmund.de

II. SIMULATION RESULTS

Initially, the storage ring was simulated by use of the Accelerator Toolbox (AT), a MatLab programming framework for accelerator studies [13–15]. The related DELTA storage ring lattice model contains all main accelerator components, including the entire setup for the OC system [16]. It consists of 54 beam position monitors which determine the beam orbit in both orbit planes simultaneously as well as 30 horizontal (horz.) and 26 vertical (vert.) orbit correction magnets (steerer) [8, 10, 17]. Based on the standard storage ring optics, 3000 uniformly distributed random sets of steerer kicks in the interval of ± 0.03 mrad (horz.) and ± 0.01 mrad (vert.) were generated for both planes. See Fig. 1 as an example. This results in 3000 closed orbit response vectors (data set no.) each with 108 entries (BPM no.) for the x,z-coupled case (see Fig. 2). For the simulation studies, the Euclidean Norm (2-norm) was used as a measure of the unweighted orbit error $\chi_{\mathrm{x,z}}$:

$$\chi_{x,z} := \|\Delta_{x,z}\|_2 = \sqrt{\sum_{i=1}^{K} (\Delta_{x,z})_i^2} \ . \tag{1}$$

It is defined as the square root of the sum of squared orbit deviations $\Delta_{x,z}^2$ for the total number K of BPMs in each orbit plane (x, z) with respect to the undisturbed orbit. The corresponding data can be summarized in histogram plots, as depicted in Fig. 3.

To simulate hardware read-back errors, artificial noise was added to the model-based data. The noise level was uniformly distributed to the ML-input and target values

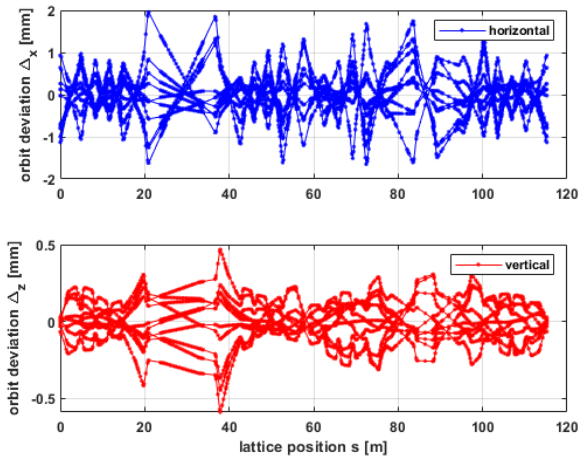

FIG. 1. Examples of closed orbit distortions for a x,z-coupled storage ring caused by 10 data sets of random steerer kicks (AT simulation, DELTA standard optics).

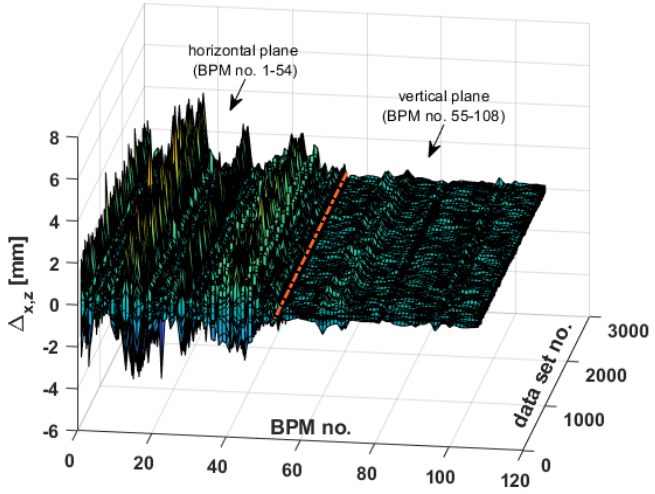

FIG. 2. Orbit response at 108 BPMs for the simulated x,z-coupled DELTA storage ring. In this example 3000 randomly disturbed orbit vectors are shown. The data sets are used as inputs for supervised training of neural networks.

with pseudo-random numbers in the range of 0% to 5% in 1%-steps. These noisy values are used as so-called 'labeled' input/target data to train fully connected shallow feed–forward NNs (see Fig. 4). The NNs consist of three neuron layers, with 108 BPM input, up to 108 hidden and 56 steerer output neurons, respectively. To enable nonlinear orbit response behavior especially for larger deviations the hyperbolic tangent function (*tanh*) was used as the neuron transfer weight-function between the input and hidden layers. The hidden and output layers are connected via a linear transfer function. Supervised training was performed using different learning algorithms. Most effective network learning methods are the scaled conjugate gradient (scg) algorithm [19] and the conjugate

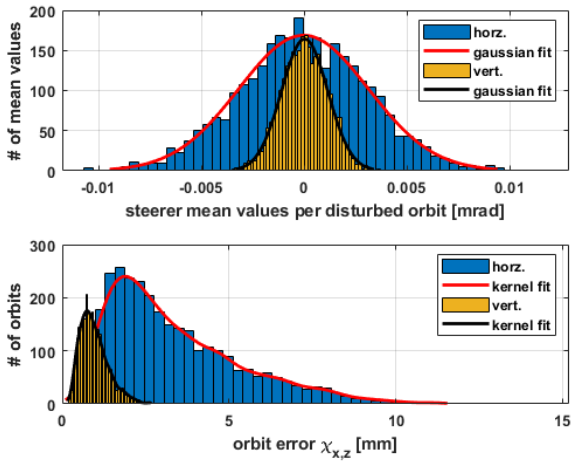

FIG. 3. Histograms of 3000 simulation data sets. Frequency distribution of the steerer strength mean values for each disturbed orbit (ML target data, top) and the corresponding frequency distribution of orbit errors (ML input data, bottom). The density fitting curves of orbit errors (red and black lines in the bottom plot) have been evaluated at 100 equally spaced points that cover the range of the data (nonparametric kernel-smoothing distribution [13], [18]).

gradient backpropagation with Fletcher-Reeves updates (cgf) [20]. Levenberg-Marquardt backpropagation [21] with Bayesian-Regularization methods [22, 23] take more computing time, but are sometimes better applicable for more challenging problems. The network training performances (often also referred to as fitness or loss-function) for a cgf-based learning algorithm with various degrees of training data noise levels are represented exemplary in Fig. 5. Usually, the fitness is rated by the mean squared normalized error performance function E_{mse} calculated at the network output:

$$E_{mse} = \frac{1}{P}\sum_{p=1}^{P}\frac{1}{N}\sum_{j=1}^{N}(o_{pj}^{steerer} - t_{pj}^{steerer})^2 \ . \qquad (2)$$

It sums up the squared differences between all target (t) and network output (o) neurons (N) for a specific number of data patterns (P). Commonly, the entire pool of patterns is divided into three data sub-sets [13]: (1) The training set (typically 80% of the total data pool) is used to fit the NN models by updating iteratively the network weights and biases. (2) The validation set (typically 10%) are 'unseen' data to verify the performance and to estimate the prediction error for an individual model selection. (3) The test data set (typically 10%) consists also of 'unseen' data kept in a so-called 'vault' to rank different NN model designs when fine-tuning model hyper-parameters. It is used for assessment of the generalization error of the final chosen model.

Fig. 5 depicts mse-scored training results for a randomly selected hidden validation sub-set of 300 recordings for various data noise levels (so-called validation

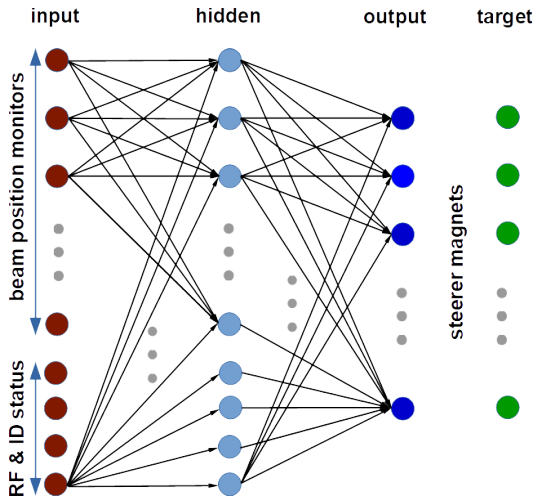

FIG. 4. Schematic view of the three-layered neural network topology to be trained for automated orbit correction. In addition to the BPM input neurons, optionally other neurons can take more components into account which influence the closed orbit data, e.g., status of the insertion devices (ID) as well as the radio frequency (RF).

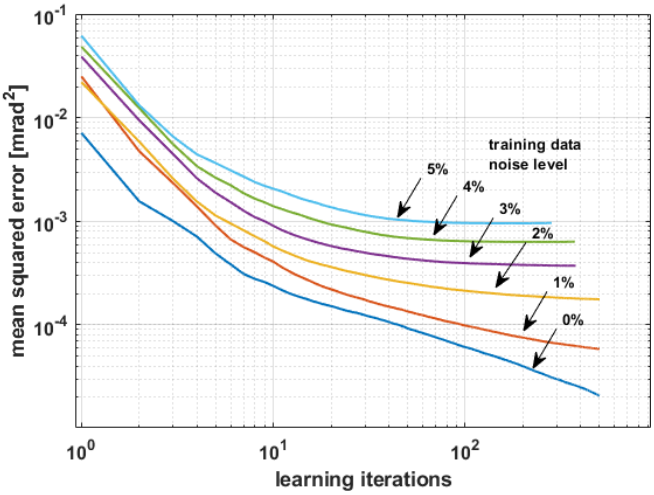

FIG. 5. Network performance functions for 'unseen' validation data sets (validation curves). Each curve refers to a hidden sub-set of 300 recordings ranking the network's performance according to the mean of squared errors (mse) for 'unseen' data. In this example, in dependence of cgf-based backpropagation learning iterations [20].

curves). It shows, that the network mse-fitness decrease with increasing number of learning iterations, but the best performance reduces also continuously with increasing noise level ('saturation effect'). For example, data noise levels larger than 3% lead to worse training results, with performance gains of less than two orders of magnitude with respect to the initial fitness. But in all cases, the falling curves indicate that the neural networks are able to learn and generalize a correlation between orbit deviations and steerer strength variations.

III. REAL MACHINE OPERATION

Based on the simulation results, a similar procedure was implemented for the real storage ring orbit correction. But now the training data were experimentally acquired during actual accelerator operation. Compared to the uncoupled case in previous real machine studies [7], at this time the orbit has been disturbed in both orbit directions simultaneously. For this purpose, all horizontally (horz.) and vertically (vert.) deflecting steerer magnets were randomly adjusted at once and subsequently the resulting closed orbit was measured at all BPM positions in both planes at the same time.

A. Data acquisition

All steerer magnets are additional coils on quadrupole yokes which can be ramped to a current of max. ±10 A, yielding to beam kicks of max. ±3 mrad horizontally and max. ±1 mrad vertically at an electron energy of 1.5 GeV. They are controlled via 12-bit digital-to-analog converters (DACs) integrated on control area bus (CAN) to serial (RS232) bus converter modules [24]. The DACs allow current changes with a granularity of 2.4 mA, which corresponds also to the minimum read-back resolution [8].

The analog capacitive multiplexed pick-up signals of the beam position monitors are read out via a mixture of I-Tech Libera [25] and Bergoz MX [26] electronics. The MX-BPMs provide the measured beam position as an analog voltage that is digitized by 12-bit analog-to-digital converters (ADCs) [27] and fed over a CAN-bus into the EPICS control system [28]. A 10 Hz low-pass filter reduces sampling noise while maintaining sufficient bandwidth for the 'slow' orbit feedback. The measuring accuracy is approx. ±5 μm, mainly limited by the resolution of the ADCs. At beam currents above 2 mA the 'slow' acquisition data from Libera BPMs are of roughly the same quality as the data from the MX-BPMs. For more detailed descriptions see [17, 29].

Since adequate experimental data, i.e., large number of randomly disturbed orbits, from an EPICS-log archive [31] were not available, a special data mining program was implemented. This program randomly varies all steerer strengths in both planes at once within intervals from typically ±200 mA up to ±500 mA. The interval limits are a compromise between risk of beam losses and minimizing relative measurement errors due to the limited steerer strength resolution of 2.4 mA. After each perturbation, the steerer strength changes and the emerging closed orbit differences in both planes are measured and recorded. Erroneous BPM readings, e.g., due to read/write time-outs and pointless outliers are directly filtered out. On average, approx. 15-20 seconds are required per single measurement cycle. That way, 4376 random steerer-BPM data combinations (corresponding to ML input/target data pairs) were recorded (see Fig. 6).

Moreover, measurements of conventional orbit response matrices for various singular positive and negative steerer kicks were carried out too. The measurements of all sources with different strength intervals were merged to a common data pool of approx. 4600 data pairs to obtain at least ten times as much training data as neurons in the NNs. The data pool noise level was estimated to approximately 2% caused by the combined error of BPM and steerer strength read–back accuracies, mainly dominated by the limited steerer strength granularity.

Similar to Fig. 3 for the simulation case, Fig. 7 depicts the measured random orbit error $\chi_{x,z}$ (ML input data) and the corresponding random steerer strength distributions (ML target data). Here, three different interval limits for the random variations ($\pm$200 mA, $\pm$300 mA, $\pm$500 mA) were combined and equally applied to the horizontal and vertical steerer magnets. With this the maximum of the orbit error distribution is located at approximately 2.7 mm horizontally and 1.3 mm vertically, whereby larger orbit errors are over-represented. The general goal is to obtain as much data as possible over a wide range of orbit errors to enable efficient correction of small to large trajectory deviations during machine operation.

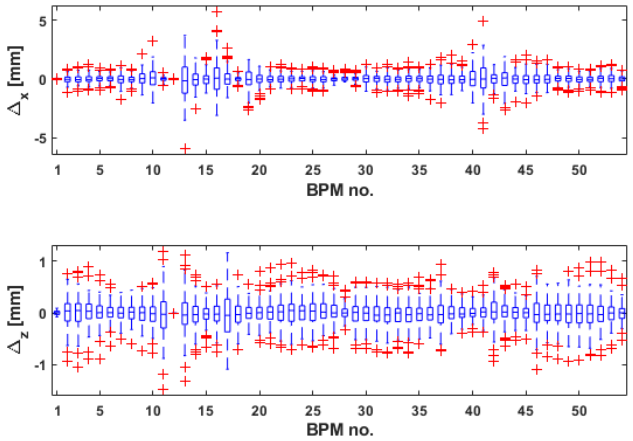

FIG. 6. Measured orbit response at 54 horizontal (top) and 54 vertical (bottom) BPM positions for the DELTA storage ring. In this example 4376 randomly disturbed orbit vectors have been measured (compare with Fig. 2). On each box, the central mark indicates the median, and the bottom and top edges of the box indicate the 25th and 75th percentiles, respectively. The whiskers extend to the most extreme data points not considered outliers, and the statistical outliers are plotted individually using the '+' symbol. These experimental data sets are used as inputs for the training of neural networks.

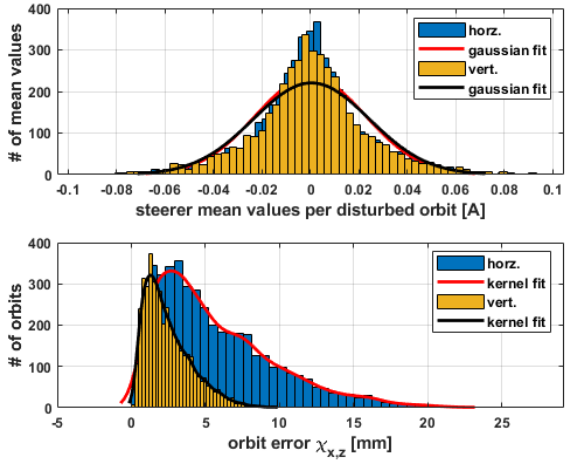

FIG. 7. Histograms of 4376 experimental data sets. Steerer strength mean values for each disturbed orbit (ML target data, top) and the corresponding frequency distribution of orbit errors (ML input data, bottom). The density fits of orbit errors (red and black lines) have been evaluated at 100 equally spaced points that cover the range of the data (nonparametric kernel-smoothing distribution [13], [18]). Compare with Fig. 3 for simulated data.

B. Weighted beam position monitors

To increase the impact of orbit deviations at more important storage ring positions (e.g., synchrotron radiation source points or the injection region) each BPM can be assigned with an individual weight factor (see Fig. 8). With $\tilde{w}_{x,z}^{BPM}$ as a diagonal matrix of BPM weight factors, the weighted orbit quality $\chi_{x,z}^{w}$ can be evaluated as a scalar quantity for both planes (x, z) by

$$\chi_{x,z}^{w} = \left\| \tilde{w}_{x,z}^{BPM} \cdot (\overrightarrow{\Delta d}_{x,z} + \tilde{R}_{x,z} \cdot \overrightarrow{\Delta I}_{x,z}) \right\|_2 . \qquad (3)$$

The goal for an orbit correction algorithm is to minimize the residual closed orbit error $\chi_{x,z}^{w}$ for arbitrary orbit deviations $\overrightarrow{\Delta d}_{x,z}$ with respect to any desired reference orbit. The right summand $\tilde{R}_{x,z} \cdot \overrightarrow{\Delta I}_{x,z}$ in equation 3 can be determined by means of a reverse neural network (see Fig. 9). The reverse NN can also be trained with the experimental data patterns (P), but now each squared network error $e_{pj}^2 = (o_{pj} - t_{pj})^2$ must be weighted by an individual BPM weight factor w_{pj}^{BPM} (see Fig.8) as follows:

$$E_{mse}^{R} = \frac{1}{P} \sum_{p=1}^{P} \frac{1}{N} \sum_{j=1}^{N} w_{pj}^{BPM} (o_{pj}^{BPM} - t_{pj}^{BPM})^2 . \qquad (4)$$

Thus, the reverse trained NN, as a representation of the orbit response matrix $\tilde{R}$, is able to determine orbit deviations $\overrightarrow{\Delta d}$ at all BPMs for given steerer strength changes $\overrightarrow{\Delta I}$. Afterwards, the weighted orbit error χ^{w} in equation 3 can be minimized with the help of a numerical

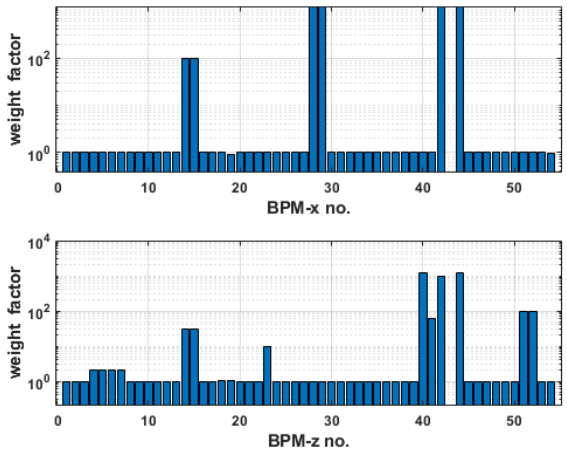

FIG. 8. Individual BPM weight factors for horizontal (top) and vertical (bottom) BPM measurements. BPM no. 43 was switched off due to hardware malfunction (reference data file: reference.200811-1).

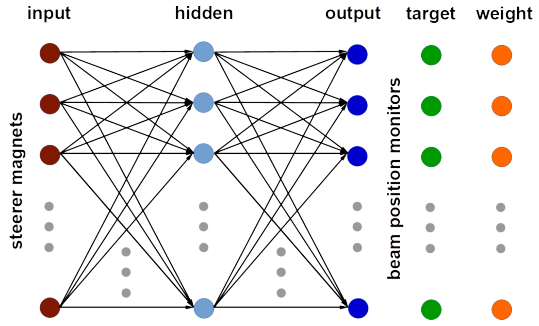

FIG. 9. Schematic view of the reverse neural network topology. Training of this network can also take weighted beam position monitors into account.

optimizer, e.g., the BFGS Quasi-Newton method [30]. In addition, the optimizer itself can also be replaced by a pre-trained NN. For this purpose, the optimizer has to pre-calculate the optimum χ^w-values for all measured orbit deviations $\overrightarrow{\Delta d}$. These data pairs again serve as labeled input/target data to train a NN as an optimizer substitute.

C. Neural network training

Since each corrector strength variation normally effects the beam amplitude at all BPM positions in the storage ring, as for the simulations, a fully connected feed-forward neural network (FFNN) was specified as the neuron network connection architecture. Thus, the NNs to be trained by the experimental data consist also of three layers (108/108/56) with a total of 272 neurons and approximately 17700 weights and biases. A schematic of the FFNN layout is shown in Fig. 10.

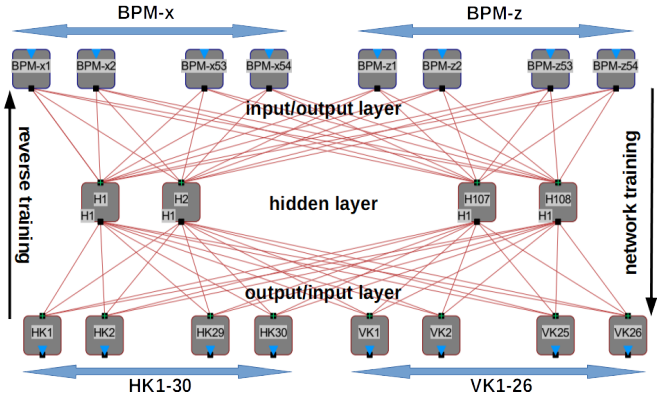

FIG. 10. Detailed layout of the neural network topology for a full x,z-coupled orbit correction at the storage ring DELTA. The input layer represents 54 BPMs for each plane, fed by measured orbit deviations. It is connected via a 'hidden' layer with the output values for 56 correction magnets (HK1-30, VK1-26). The correction considers both transversal coordinates (x, z) as well as their coupling. In total the network consists of approx. 17700 connections (red lines, only partially shown). For reverse training the input and output layers have been swapped (see Fig. 4 and Fig. 9). Figure partly created with 'MemBrain' [32].

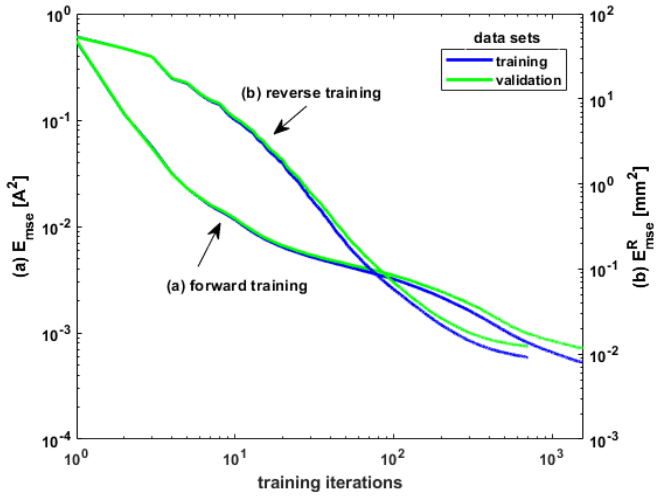

FIG. 11. Neural network training (see Fig. 4 and Fig. 9) with experimental training data (blue) and verification of the neural network with an additional 'unseen' validation test data set (green). In these examples a scaled conjugate gradient (scg) backpropagation algorithm was applied. A forward training performance of $7.3 \cdot 10^{-4}\,\mathrm{A}^2$ was reached with no significant improvement after approx. 1600 iterations. The reverse training achieved a network error of $1.2 \cdot 10^{-2}\,\mathrm{mm}^2$ after about 700 iterations. In all cases the neural network training errors were reduced approximately three orders of magnitude related to the initial values.

The supervised network training was carried out with various conjugate gradient backpropagation learning algorithms. Most effective learning was achieved with scaled conjugate gradient (scg) based algorithms [19].

Typical forward and reverse training curves for pure training data (blue curves) and the related validation data sets (green curves) are shown in Fig. 11. In both cases, the network output error is reduced continuously, mainly limited by the data noise level. Best forward validation performance (E_{mse}-value) of $7.3 \cdot 10^{-4}\,\mathrm{A}^2$ was reached after 1600 scg-training iterations (often also referred to as epochs) applying a full batch (all patterns) training. The reverse training reduced the network output error (E^R_{mse}-value) to $1.2 \cdot 10^{-2}\,\mathrm{mm}^2$ after 700 iterations. For both cases, the network's fitness gains approximately three orders of magnitude compared to the starting values, which indicates sufficient fitness performance and is comparable with the simulation results (see Fig. 5). Hence, also for the experimental data, NNs are able to learn and generalize the correlation between orbit deviations and the related steerer strength variations.

Finally, the scg-trained NNs, which correspond best to a machine learned orbit correction model, with gaining performances at a minimum of three orders of magnitude, were tested to predict the steerer strengths settings to compensate real orbit deviations. Through iterative use of the sign inverted values from the network output (predicted steerer strengths changes), the trained NNs were able to correct successively any randomly disturbed closed orbit. This was verified by dedicated benchmark tests.

IV. BENCHMARK RESULTS

The performance of the machine learning based orbit correction program was benchmarked against a recently implemented numerical-based OC approach [11, 12] at different reference conditions. The tests considered actual reference settings, which define the currently valid reference orbit and weight factors (wf) of the used numbers K of BPMs (see Fig. 8). Various arbitrary steerer induced orbit errors have been generated (a–d) in both orbit planes respectively (hk/vk), which are indicated by the legends in the figures. The benchmark measurements are shown see Fig. 12 (ML-based) and Fig. 13 (numerical-based) separately for each orbit plane.

In addition, typical but not pre-trained sources for orbit disturbances have been provoked. This includes unmatched closed orbit bumps (e.g., injection dc-bump), strong sextupole strength changes (SF/SD) or ramping of insertion devices (e.g., U250). The benchmark results are shown in Fig. 14 (ML-based) and Fig. 15 (numerical-based) for each plane separately.

The residual orbit quality $\chi^w_{x,z}$ is scored by the weighted root mean squared value (wrms) over all K BPMs in both orbit planes (x, z):

$$\chi^w_{x,z} := \sqrt{\frac{1}{K}\sum_{i=1}^{K}\left(w^{BPM}_{x,z}\cdot\Delta_{x,z}\right)^2_i}\,. \qquad (5)$$

The individual start wrms-errors $\chi^w_{x,z}$ (a–j) for both measurement methods are slightly different, mainly caused by a wiggler magnet strength drift during data acquisition.

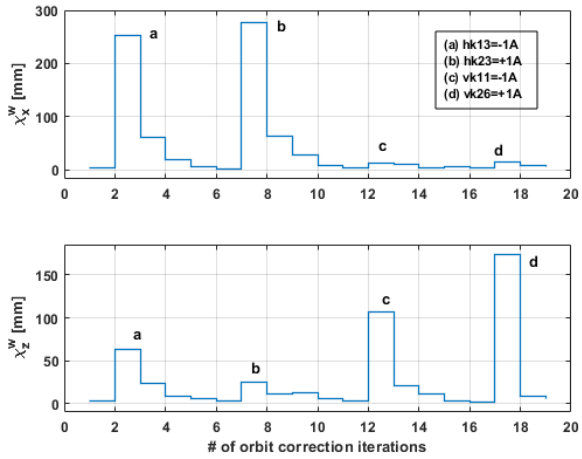

FIG. 12. Weighted rms orbit error $\chi^w_{x,z}$ for different steerer (hk/vk) induced orbit disturbances (a-d) compensated iteratively by the ML-based OC program. Due to x,z-coupling the provoked deviations appear in both orbit planes. A total of 18 steps were required to compensate for all disturbances (a-d). In comparison to Fig. 13, similar final residual orbit errors are achieved in significantly fewer iterations.

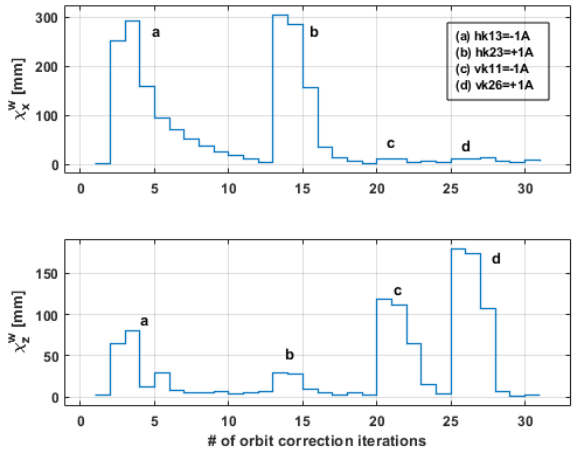

FIG. 13. Weighted rms orbit error $\chi^w_{x,z}$ to benchmark the orbit correction quality and convergence for a conventional, numerical-based method [11, 12]. The correction was performed iteratively for different steerer (hk/vk) caused orbit distortions (a-d). As in Fig. 12, orbit deviations appear in both orbit planes because of x,z-coupling. A total of 30 steps were required to compensate for all disturbances (a-d).

As can be seen from the graphs both OC programs, the machine learning based version as well as the conventional numerical-based approach, worked similarly stable and they were able to compensate all orbit disturbances without any beam losses. The ML-based OC needs approximately 2–4 orbit correction iterations to equalize the

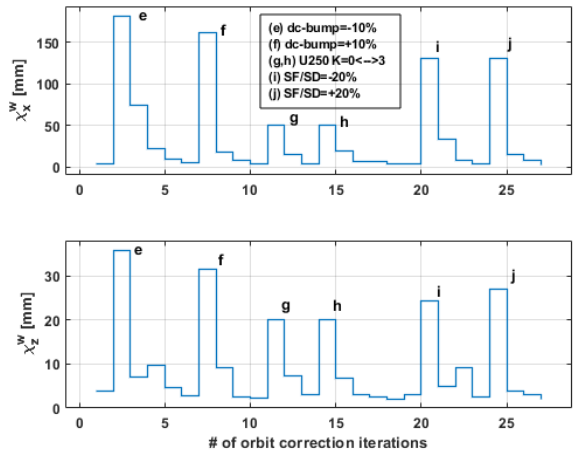

FIG. 14. Individual ML-based correction steps to compensate orbit deviations caused by different error sources (a-j) which were not included in the training data sets. Although these types of error sources were not considered during NN training, all disturbances (a-j) could be compensated in a total of 26 steps.

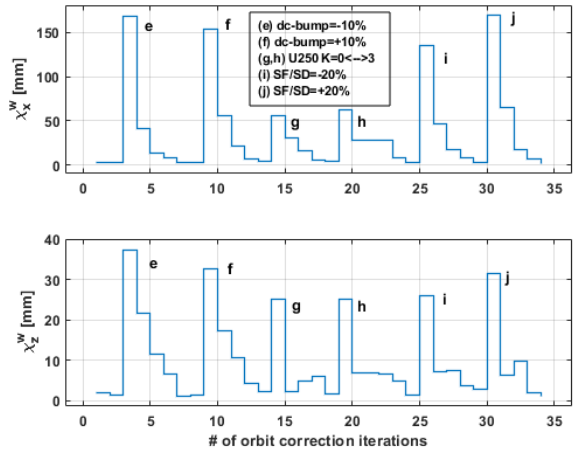

FIG. 15. Correction for different scenarios of orbit deviations (a-j) performed with a conventional orbit correction program [11, 12]. In this case, a total of 33 steps were required to compensate for all perturbations (a-j). Compare with Fig. 14.

individual provoked orbit deviations. Even distortions (e–j) which were not trained during supervised learning have been compensated with analogous quality. After each provoked error the residual weighted orbit error converged to less than 3 mm which could be improved by adding more training data in the range with smaller orbit deviations (see Fig. 7). In direct comparison, the conventional OC method requires more orbit correction iterations to compensate the same provoked orbit disturbances. The residual weighted orbit error converged also to less than 3 mm, but over all, in these benchmark examples the standard OC version needs 63 steps (see Fig. 13 and Fig. 15) compared to 44 steps for the ML-based implementation (see Fig. 12 and Fig. 14).

V. SUMMARY AND OUTLOOK

A machine learning-driven orbit correction has successfully been implemented at the 1.5–GeV electron storage ring of the DELTA accelerator facility. It has been shown that ML-based implementations are competitive with classical SVD-like numerical approaches. The achieved remaining orbit error is similar to the results of these standard correction algorithms. In general, ML-based methods require fewer correction steps which leads to significantly faster orbit correction convergence. Since ML techniques based on training with real machine data, this method automatically incorporates storage ring imperfections (e.g., alignment errors) and non-linearities (e.g., magnetic fringe fields) during beam position controlling. Furthermore, it has been demonstrated that NNs were also able to cope with beam disturbances that had not been trained previously. In addition, even changes of BPM offsets, e.g. due to the realignment of individual lattice magnets, can be taken into account simply by editing the orbit reference data file. Therefore retraining of the entire neural network is not required. In general, once trained, the NN-based application showed high reliability, numerical stability and robustness.

Despite ML-based OC being competitive, there is still potential for improvements. For example, at DELTA large beam amplitudes at sextupole magnets integrated into the quadrupole magnets generate strong orbit kicks which can be of the same order as steerer kicks. So far, this effect was not taken into account, but could also be included due to additional dedicated 'sextupole neurons'. Another major upgrade would be the introduction of adaptive training methods. In this case, the NNs would be constantly supplied with current measurement data and dynamically kept up to date by so-called 'training on the fly' techniques. Finally, the integration of the already installed weak but fast steerer magnets could supplementary be helpful especially for minor orbit correction steps.

ACKNOWLEDGMENTS

I would like to thank all colleagues of the DELTA team for many helpful advises and suggestions as well as for providing sufficient data mining time during accelerator shifts. Special thanks to Stephan Kötter for plenty stimulating discussions and Andrè Althaus for his support with all control system issues.

[1] A. Edelen *et al.*, "Opportunities in Machine Learning for Particle Accelerators", arXiv: 1811.03172 (2018)

[2] Edelen, Auralee and Neveu, Nicole and Frey, Matthias and Huber, Yannick and Mayes, Christopher and Adelmann, Andreas, "Machine learning for orders of magnitude speedup in multiobjective optimization of particle accelerator systems", Phys. Rev. Accel. Beams, Vol. 23, pp. 044601, 2020. doi:10.1103/PhysRevAccelBeams.23.044601

[3] D. Schirmer, "Intelligent Controls for the Electron Storage Ring DELTA", in *Proc. 9th Int. Particle Accelerator Conf. (IPAC'18)*, Vancouver, Canada, Apr.-May 2018, pp. 4855–4858. doi:10.18429/JACoW-IPAC2018-THPML085

[4] M. Tolan, T. Weis, C. Westphal, and K. Wille, "DELTA: Synchrotron light in nordrhein-westfalen", *Synchrotron Radiation News*, Vol. 16, pp. 9-11, Mar. 2003. doi:10.1080/08940880308603005

[5] S. Khan *et al.*, "Coherent Harmonic Generation at DELTA: A New Facility for Ultrashort Pulses in the VUV and THz Regime", in *Synchrotron Radiation News 24*, 18 (2011). doi:10.1080/08940886.2011.618092

[6] S. Khan *et al.*, "Generation of Ultrashort and Coherent Synchrotron Radiation Pulses at DELTA", *Synchrotron Radiation News*, Vol. 26, pp. 25-29, May 2013. doi1:0.1080/08940886.2013.791213

[7] D. Schirmer, "Orbit Correction with Machine Learning Techniques at the Synchrotron Light Source DELTA", in *Proc. of 17th Int. Conf. on Accelerator and Large Experimental Physics Control Systems (ICALEPCS'19)*, New York, USA, Oct. 2019, p. 1426. doi:10.18429/JACoW-ICALEPCS2019-WEPHA138

[8] D. Zimoch, "Implementierung eines Orbitkorrektursystems an der Synchrotronstrahlungsquelle DELTA", dissertation, Phys. Dept., TU Dortmund, Germany, 2002.

[9] B. Keil, "A Unified Distributed DSP-Based Beam Diagnostics and Global Feedback System for Ramped Electron Storage Rings: Development, Construction and Applications", dissertation, Phys. Dept., TU Dortmund, Germany, 2003.

[10] M. Grewe, "SVD-basierte Orbitkorrektur am Speicherring Delta", dissertation, Phys. Dept., TU Dortmund, Germany, 2005.

[11] S. Kötter, B. Riemann, and T. Weis, "Status of the Development of a BE-Model-Based Program for Orbit Correction at the Electron Storage Ring DELTA", in *Proc. 8th Int. Particle Accelerator Conf. (IPAC'17)*, Copenhagen, Denmark, May 2017, pp. 673–675. doi:10.18429/JACoW-IPAC2017-MOPIK065

[12] S. Kötter, A. Glaßl, B. D. Isbarn, D. Rohde, M. Sommer, and T. Weis, "Evaluation of an Interior Point Method Specialized in Solving Constrained Convex Optimization Problems for Orbit Correction at the Electron Storage Ring at DELTA", in *Proc. 9th Int. Particle Accelerator Conf. (IPAC'18)*, Vancouver, Canada, Apr.-May 2018, pp. 3507–3510. doi:10.18429/JACoW-IPAC2018-THPAK114

[13] MATLAB/SIMULINK and Neural Network, Fuzzy Logic, Genetic Algorithm Toolboxes, Release 2017b, The MathWorks, Inc., Natick, Massachusetts, United States.

[14] ATcollab, http://atcollab.sourceforge.net/index.html.

[15] A. Terebilo, "Accelerator Modeling with Matlab Accelerator Toolbox", in *Proc. of the 2001 Particle Accelerator Conference (PAC'01*, 18–22 June 2001, Chicago, USA, pp. 3203–3205. doi:10.1109/PAC.2001.988056

[16] D. Schirmer and A. Althaus, "Integration of a Model Server into the Control System of the Synchrotron Light Source DELTA", in *Proc. of 17th Int. Conf. on Accelerator and Large Experimental Physics Control Systems (ICALEPCS'19)*, New York, USA, Oct. 2019, p. 1421. doi:10.18429/JACoW-ICALEPCS2019-WEPHA137

[17] A. Jankowiak, "Strahldiagnose und Closed-Orbit-Charakterisierung mit HF-Strahllagemonitoren am Beispiel der Synchrotronstrahlungsquelle DELTA", dissertation, Dortmund University, 1999.

[18] https://en.wikipedia.org/wiki/Kernel_density_estimation

[19] Moller, M. F., "A scaled conjugate gradient algorithm for fast supervised learning"Neural Networks, Vol. 6, 1993, pp. 525–533.

[20] Fletcher, R. and Reeves, C. M., "Function minimization by conjugate gradients", Computer Journal, Vol. 7, 1964, pp. 149–154.

[21] Hagan, M. T., H. B. Demuth and M. H. Beale, "Neural Network Design", Boston, MA: PWS Publishing, 1996.

[22] F. Dan Foresee and Martin T. Hagan, "Gauss-Newton Approximation to Bayesian Learning", in *Proc. Int. Conf. on Neural Networks (ICNN'97)*, Jun. 1997, Vol. 3, pp. 1930–1935. doi:10.1109/ICNN.1997.614194

[23] MacKay, David J. C. "Bayesian interpolation", Neural computation. Vol. 4, No. 3, 1992, pp. 415–447.

[24] esd-electronics system design gmbh, "can-ccom4 Hardware-Handbuch", CAN-CCOM4 Hardware Rev. 2.0, Hannover, Germany, 1994.

[25] Instrumentation Technologies, http://www.i-tech.si.

[26] J. Bergoz, "Multiplexed Beam Position Monitor User's Manual", Bergoz Instrumentation, Rev. 1.5.4.

[27] esd-electronics system design gmbh, "can-cai812 Hardware-Handbuch", CAN-CAI812 Hardware Rev. 2.0, Hannover, Germany, 1993.

[28] Experimental Physics and Industrial Control System (EPICS), https://epics-controls.org

[29] P. Hartmann, J. Fuersch, D. Schirmer, T. Weis, and K. Wille, "Experience with Libera Beam Position Monitors at DELTA", in *Proc. 8th European Workshop on Beam Diagnostics and Instrumentation for Particle Accelerators (DIPAC'07)*, Venice, Italy, May 2007, paper TUPB21, pp. 111–113.

[30] Broyden-Fletcher-Goldfarb-Shanno (BFGS), https://en.wikipedia.org/wiki/Broyden-Fletcher-Goldfarb-Shanno_algorithm

[31] D. Schirmer, A. Althaus, P. Hartmann, D. Rohde, "Control System Projects at the Electron Storage Ring DELTA", in *Proc. of 17th Int. Conf. on Accelerator and Large Experimental Physics Control Systems (ICALEPCS'17)*, Barcelona, Spain, Oct. 2017, p. 1361. doi:10.18429/JACoW-ICALEPCS2017-THPHA013

[32] MemBrain Neural Network Simulator, https://membrain-nn.de/main_en.htm